Effects of Large Scale High Freestream Turbulence and Exit Reynolds Number on Turbine Vane Heat Transfer in a Transonic Cascade

Shakeel Nasir
Jeffrey S. Carullo
Wing-Fai Ng
Karen A. Thole
Hong Wu

Department of Mechanical Engineering,
Virginia Polytechnic Institute and State University,
Blacksburg, VA 24061

Luzeng J. Zhang
Hee Koo Moon

Heat Transfer Department,
Solar Turbines Inc.,
San Diego, CA 92186

This paper experimentally and numerically investigates the effects of large scale high freestream turbulence intensity and exit Reynolds number on the surface heat transfer distribution of a turbine vane in a 2D linear cascade at realistic engine Mach numbers. A passive turbulence grid was used to generate a freestream turbulence level of 16% and integral length scale normalized by the vane pitch of 0.23 at the cascade inlet. The base line turbulence level and integral length scale normalized by the vane pitch at the cascade inlet were measured to be 2% and 0.05, respectively. Surface heat transfer measurements were made at the midspan of the vane using thin film gauges. Experiments were performed at exit Mach numbers of 0.55, 0.75, and 1.01, which represent flow conditions below, near, and above nominal conditions. The exit Mach numbers tested correspond to exit Reynolds numbers of 9×10^5, 1.05×10^6, and 1.5×10^6 based on a vane chord. The experimental results showed that the large scale high freestream turbulence augmented the heat transfer on both the pressure and suction sides of the vane as compared to the low freestream turbulence case and promoted a slightly earlier boundary layer transition on the suction surface for exit Mach 0.55 and 0.75. At nominal conditions, exit Mach 0.75, average heat transfer augmentations of 52% and 25% were observed on the pressure and suction sides of the vane, respectively. An increased Reynolds number was found to induce an earlier boundary layer transition on the vane suction surface and to increase heat transfer levels on the suction and pressure surfaces. On the suction side, the boundary layer transition length was also found to be affected by increase changes in Reynolds number. The experimental results also compared well with analytical correlations and computational fluid dynamics predictions.
[DOI: 10.1115/1.2952381]

Keywords: gas turbine, vane, high turbulence, Reynolds number, heat transfer, thin film gauge

Introduction

One way to increase the cycle efficiency of a gas turbine engine is to operate at higher turbine inlet temperatures (TITs). In most engines, the TITs have increased to be well above the metallurgical limit of engine components. Cooling of turbine engine components (blades and vanes) is a widely used technique that allows higher TITs by maintaining material temperatures within acceptable limits. Accurate turbine section heat transfer modeling can lead to an optimized cooling design and therefore higher TITs.

Numerical modeling of heat transfer through turbine passages is a challenge as it is complicated by several factors such as Reynolds number, Mach number, combustor-generated high freestream turbulence, turbulence length scale, hot streaks, and secondary flows, just to name a few. The efforts of this work are to experimentally and numerically investigate the effects of large scale high freestream turbulence on first stage turbine vane heat transfer at realistic engine Mach number conditions.

Contributed by the Turbomachinery Division of ASME for publication in the JOURNAL OF TURBOMACHINERY. Manuscript received September 18, 2007; final manuscript received October 21, 2007; published online February 3, 2009. Review conducted by David Wisler. Paper presented at the 2007 ASME International Mechanical Engineering Congress (IMECE2007), Seattle, WA, November 10–16, 2007.

Summary of Past Literature. While measuring the turbulence level in a gas turbine is extremely difficult, researchers have found that combustion systems typically produce turbulence levels between 7% and 30% [1,2]. Ames et al. [3] reported that the exit turbulence levels depend on combustor core flow to vane inlet contraction ratio and the residence time of the flow in the combustor.

Several research groups have performed heat transfer experiments on turbine vane geometries in low speed cascade facilities. Ames et al. [3–5] investigated the effects of freestream turbulence and length scale on vane heat transfer at different exit Reynolds number conditions. In all these studies with different turbulence generators, Ames et al. observed that turbulence augmented the heat transfer in the laminar region with the highest augmentation in the stagnation region and on the pressure side. An earlier transition to a turbulent boundary layer was also observed on the suction side of the vane when the turbulence level was increased. The length scale effect was also observed with the augmentation on pressure side heat transfer increased as the length scale was decreased. Radomsky and Thole [6] documented surface heat transfer and the highly turbulent flow field around a scaled-up stator vane. Their observations of the heat transfer augmentation on the vane surface were also consistent with Ames [4].

Several experimental studies have also been performed in transonic cascade facilities to investigate the effect of freestream tur-

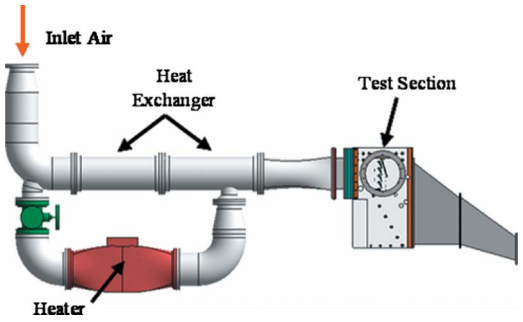

Fig. 1 Virginia Tech transonic cascade wind tunnel

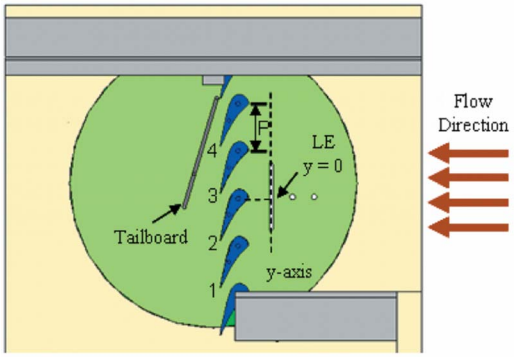

Fig. 2 Cascade diagram showing the vanes and the axis orientation for measurements with the traverse

bulence, Mach number, and exit Reynolds number on vane heat transfer. Nealy et al. [7] found that turbulence augmented heat transfer on the vane surface. He also found that an increase in Reynolds number increased heat transfer levels on the vane surface and the exit Mach number controlled the heat transfer distribution on the suction side of the vane. Arts and Lambert de Rouvroit [8] found augmentation levels of up to 100% on the laminar portion of the vane subjected to 6% turbulence levels.

Hoffs et al. [9] investigated the effects of Reynolds number and turbulence on smooth vane heat transfer in a high speed facility and found that the boundary layer on the pressure side started transition with an increase in the heat transfer coefficient near the trailing edge. Bunker [10] also investigated the effects of high freestream turbulence (13%) and Reynolds number on the vane heat transfer in a linear cascade. He found that pressure side heat transfer was less affected by turbulence but showed a consistent increase with turbulence over the whole pressure surface. He found that increased turbulence hastened suction side transition. Bunker also found that heat transfer on the suction side of the vane aft of transition followed a proportionality of $Re^{1.0}$.

Experimental Setup and Instrumentation

Wind Tunnel Facility. The two-dimensional Virginia Tech transonic cascade wind tunnel, shown in Fig. 1, is a blowdown facility that is capable of sustaining a constant inlet pressure in the test section for up to 25 s. Prior heat transfer research that has been performed in this facility includes work of Carullo et al. [11], Nix et al. [12], Holmberg and Diller [13], Smith et al. [14], and Popp et al. [15]. Air is supplied from high pressure air tanks that are charged up to 1380 kPa (200 psi (gauge)) prior to testing. A control valve regulates the flow from the air tanks to the test section. Cascade inlet pressures range from 20.7 kPa (3 psi (gauge)) to 69.0 kPa (10 psi (gauge)) depending on the objective test conditions. Between the control valve and the test section, the air passes through a passive heat exchanger, which heats the cascade inlet flow up to 120°C. After the air passes through the heat exchanger, the air goes through a contraction and enters the test section before being exhausted to the atmosphere.

The turbine vane tested in these experiments is similar in geometry to a first stage turbine vane for a small industrial gas turbine. The vane was scaled one and a half times so that the nominal exit Reynolds number would be at the desired value. Table 1 summarizes the geometry of the turbine vane.

Table 1 Vane geometry

Chord	91.2 mm (3.59 in.)
Axial chord	50.0 mm (1.97in.)
Pitch	83.0 mm (3.27in.)
Span	152.4 mm (6.00 in.)
Inlet and exit angles	0 deg and 73.5 deg

A diagram of the vane cascade is provided in Fig. 2. From the vane geometry and the test section size, the vane cascade consists of four full vanes and two partial vanes, which result in four full passages and one partial passage. A tailboard placed at the vane exit angle aids in creating periodic flow through the cascade. The full vanes are numbered starting from the lower bottom of the cascade, with Vane 2 being the vane that is fully instrumented to make static pressure and heat transfer measurements. The slot located 0.45C upstream of the cascade is used to measure the turbulence and velocity distributions at the inlet of the cascade.

Static Pressure Measurements. To calculate the isentropic Mach number distribution on the vane surface, the turbine vane was instrumented with static pressure taps placed at the midspan of the vane. Vane 2 was instrumented with 7 taps on the pressure side, 18 taps on the suction side, and 1 tap near the leading edge. Static pressure taps were also instrumented on the suction side of Vane 1 and on the pressure side of Vane 3 to check the periodicity of the flow. The static pressure measurements were made through experiments conducted independently of the heat transfer experiments. In addition to calculating the isentropic Mach number distribution, the acceleration parameter distribution on the vane surface was calculated.

Static pressure taps on the end wall of the cascade were used to measure the inlet and exit static pressures and characterize the inlet and exit flows. Fourteen inlet static taps were located 0.45C upstream of the vane passages and 14 exit static taps were located 0.45C downstream of the vane passages. Figure 3 provides typical cascade inlet temperature and inlet and exit Mach number time histories during a blowdown test run.

Heat Transfer Measurements. Heat transfer measurements were made with thin film gauges that allow for high spatial resolution measurements on the vane surface with minimal flow dis-

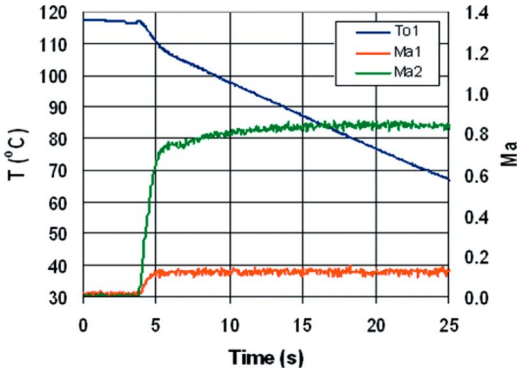

Fig. 3 Cascade inlet temperature and Mach number history

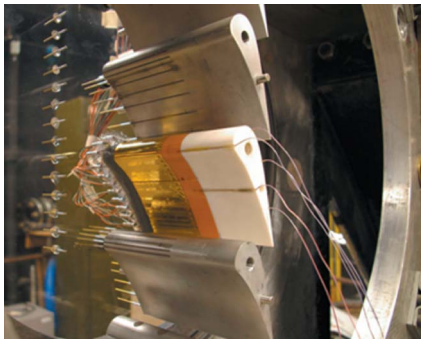

Fig. 4 Photograph of thin film gauges in wind tunnel

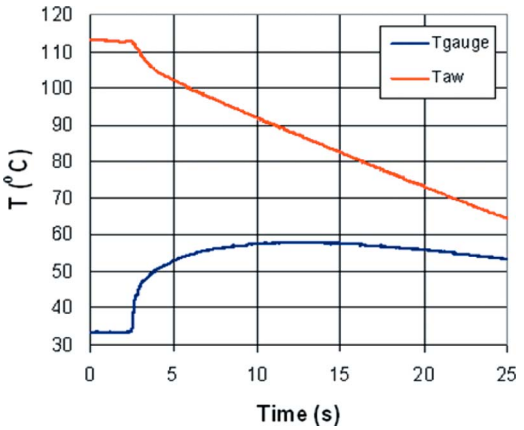

Fig. 5 Typical vane surface and adiabatic wall temperatures history

ruption. Thin film gauges were originally developed by Schultz and Jones [16], and variations of the original design were used by Doorly and Oldfield [17] and Dunn [18]. The thin film gauges that were used in these experiments are two-layer thin film gauges similar to the gauges developed by Doorly and Oldfield [17]. The gauges were manufactured according to the procedure described by Joe [19].

Each thin film gauge consists of a 3.18 mm (0.125 in.) long platinum sensor attached to copper leads, which are sputtered to a Kapton sheet that is (k=0.12 W/m K) 50 μm thick. The Kapton sheet with the gauges is attached to a vane manufactured from a low thermal conductivity ceramic material, Macor (k =1.46 W/m K). A photograph of the gauges installed on the vane is shown in Fig. 4. Forty-three thin film gauges were instrumented on the vane, with platinum sensors placed at the midspan of the vane.

Thin film gauges are used to measure a change in temperature on the surface of the vane. The platinum sensor of the thin film gauge changes resistance with temperature and is therefore calibrated for temperature coefficients of resistivity prior to testing. Since the gauge changes resistance with temperature, the gauge is used as one arm of a Wheatstone bridge circuit. The Wheatstone bridge used in these experiments is described by Joe [19]. The change in voltage across the bridge during the experiment is sampled at 1 kHz during the experiment using a 16 bit NI SCXI-1600 data acquisition system. The data from up to 31 gauges can be recorded in this facility during a single test.

To reduce the heat transfer data, several steps must be taken. The voltage output from each Wheatstone bridge is converted into a surface temperature using the gauge calibration and basic Wheatstone bridge operating principles. Next, the heat flux for each gauge is calculated by using a finite-difference code developed by Cress [20]. The finite-difference code uses the time history of the surface temperature of the gauge as a boundary condition and solves the one-dimensional transient heat conduction equation. Over the majority of the vane, the conduction is assumed to be semi-infinite since Macor conducts heat very slowly. Near the trailing edge, the heat flux is calculated over a finite material thickness, with the surface temperature measured by the gauges on each side of the vane used as the boundary conditions to calculate heat flux. Once the heat flux is determined, the heat transfer coefficient can then be calculated by using

$$h = \frac{q''}{(T_{\text{aw}} - T_{\text{gauge}})} \tag{1}$$

where the adiabatic wall temperature is defined as

$$T_{\text{aw}} = T_{o1}\left(\frac{1 + r_c\frac{\gamma-1}{2}\text{Ma}^2}{1 + \frac{\gamma-1}{2}\text{Ma}^2}\right) \tag{2}$$

It was assumed that the boundary layer was turbulent everywhere, so a recovery factor of $r_c = \text{Pr}^{1/3}$ was applied to all of the gauges. The heat transfer coefficient can then be nondimensionalized by calculating the Nusselt number as

$$\text{Nu} = \frac{hC}{k_a} \tag{3}$$

The heat transfer coefficient can also be nondimensionalized in terms of the Stanton number given by

$$\text{St} = \frac{h}{\rho_L U_L C_p} \tag{4}$$

Figure 5 shows typical vane surface temperature and adiabatic wall temperature time histories, and Fig. 6 shows the calculated heat flux and heat transfer coefficient time histories during a blowdown test run.

Uncertainty Analysis. The experimental uncertainty of the heat transfer measurements was calculated by using the perturbation method described by Moffat [21]. The analysis took into account the bias error and precision error. An uncertainty was calculated for each gauge at every test condition. The total uncertainty of the heat transfer coefficient for the gauges ranged between $\pm$8.5% and $\pm$11.0% with the bias error contributing to the majority of the total uncertainty. For each test condition, measurements were performed at least three times to establish repeatability.

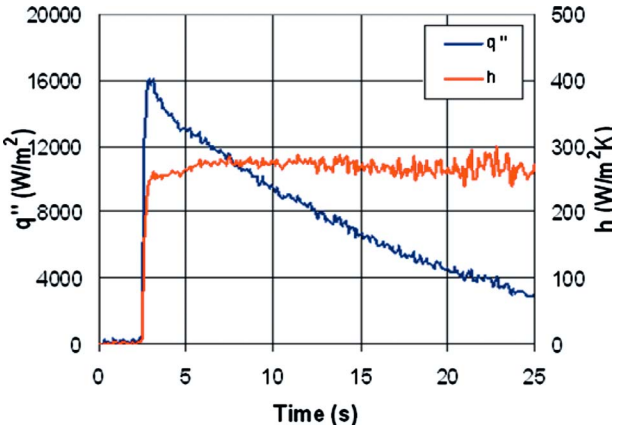

Fig. 6 Typical vane surface heat flux and heat transfer coefficient history

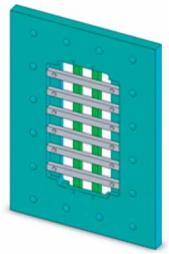

Fig. 7 Square mesh turbulence grid

Turbulence Generation

To generate freestream turbulence levels of 16%, a passive square mesh turbulence grid was used. A schematic of the turbulence grid is provided in Fig. 7. The grid design was based on the correlations reported by Baines and Peterson [22] and on research performed by Nix et al. [23] on turbulence grids in the cascade wind tunnel. The square mesh grid has bar widths of 1.91 cm (0.75 in.) and is spaced to create 3.81×3.81 cm^2 (1.5×1.5 in.^{2}) square openings. The porosity of the square mesh grid is 52%.

The location of turbulence grid relative to the test section is provided in Fig. 8. The turbulence grid is oriented so that the flow is perpendicular to the grid bars. The mesh grid was placed downstream of the two-dimensional contraction with a spacer (1.25 in. thick) placed between the contraction and test section. The nondimensional streamwise distance from the turbulence grid to the turbulence measurement slot is given by $x/B=16$.

The velocity fluctuations in the streamwise direction were measured using a single hot-film probe with a 50 μm diameter and roughly 1.5 mm long film that was connected to a constant-temperature anemometer. Hot-film data were sampled for approximately 1.3 s at 100 kHz and filtered at 40 kHz. The hot-film probe was discretely traversed over one vane pitch along the vertical slot, as shown in Fig. 2. The turbulence intensity and integral turbulence length scales were calculated at each measurement location. The turbulence length scales were calculated using the methods described by Nix et al. [23] who applied Taylor's hypothesis of frozen turbulence. The turbulence levels and length scales were measured for the square mesh grid and a base line case where no turbulence grid was installed in the tunnel. The turbulence intensity and the normalized integral length scale distributions along the vane inlet pitch are provided in Figs. 9 and 10, respectively. The summary of turbulence measurements is provided in Table 2.

To check the uniformity of the inlet flow to the vane passages downstream of the turbulence grid, a Kiel probe was continuously traversed at low speed along the measurement slot shown in Fig. 2. A velocity ratio was obtained by dividing the velocity measured from the Kiel probe by the velocity measured from a stationary Pitot probe. The velocity ratio for the square mesh grid and a base line configuration tested is provided in Fig. 11.

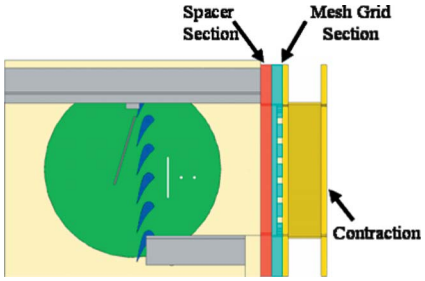

Fig. 8 Square mesh turbulence grid location relative to the test section

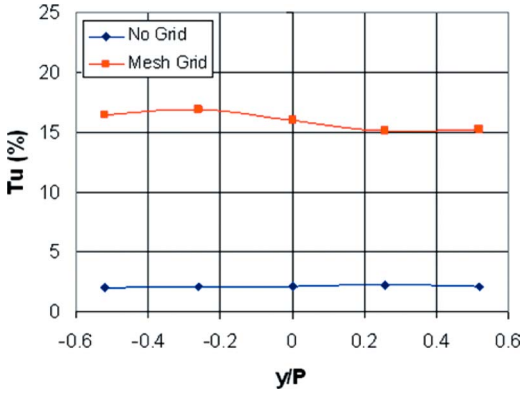

Fig. 9 Turbulence intensity along the inlet pitch

Vane Static Pressure Distribution

Figure 12 shows the local Mach number distributions on the vane surface for three exit Mach number conditions. The Mach number distribution varies smoothly along the pressure side and does not exhibit any velocity peak downstream of the stagnation region. The flow on the suction side continuously accelerates up to the geometric throat area ($s/C=0.51$). The exit Mach 0.6 and 0.8

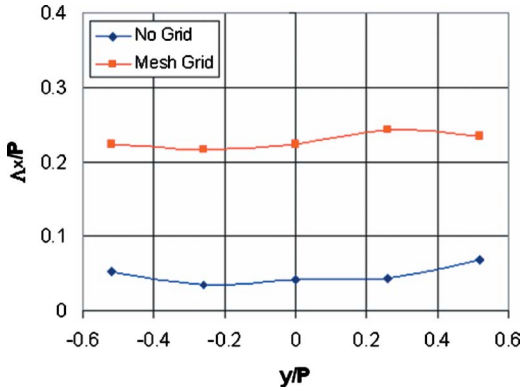

Fig. 10 Integral length scale along the inlet pitch

Table 2 Summary of grid generated turbulence

	Tu intensity	Length scale (Λ_x/P)	Turbulent KE (k/U_1^2)
Base line	2%	0.05	0.0002
Mesh grid	16%	0.23	0.0128

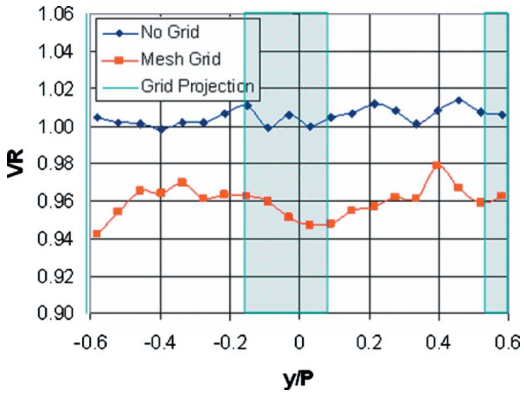

Fig. 11 Velocity ratio distribution along the inlet pitch

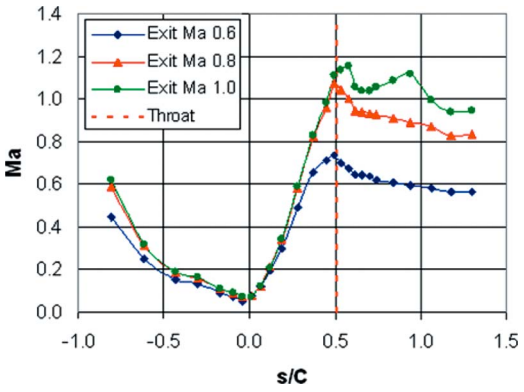

Fig. 12 Local Mach number distribution

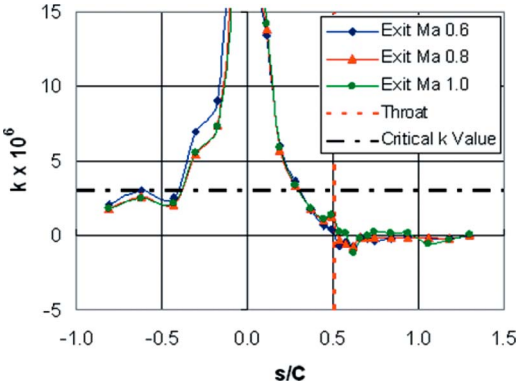

Fig. 14 Acceleration parameter distribution

cases decelerate immediately after the throat, whereas the exit Mach 1.0 case continues to accelerate and becomes supersonic. A trailing edge shock from the adjacent vane impinging on the suction surface ($s/C=0.58$) causes the multiflow decelerations after the throat for the exit Mach 1.0 case.

The periodicity of the flow at exit Mach 0.8 is provided in Fig. 13. The flow periodicity is shown by comparing the local Mach number distribution over the vane surfaces. The suction sides of Vanes 1 and 2 show the same local Mach number distributions over the majority of the suction surface. There is a slight variation in the local Mach numbers near the geometric throat. The pressure side of Vanes 2 and 3 shows almost identical local Mach number distributions with very small variation downstream of the stagnation region.

The distribution of acceleration parameter, k, on the vane surface for each exit Mach number is provided in Fig. 14. A positive acceleration parameter indicates that the flow is accelerating and a negative value indicates that the flow is decelerating. On the pressure side of the vane, the acceleration parameter for exit Mach 0.6 case barely reaches the critical value of 3×10^{-6} after $s/C=-0.43$. This critical value of k has been observed by Jones and Launder [24] and Mayle [25] as a criterion for boundary layer relaminarization.

Vane Heat Transfer Distribution

Test Conditions. Heat transfer measurements were performed at exit Mach numbers of 0.55, 0.75, and 1.01. The turbulence levels were varied between 2% and 16% at each exit Mach number. The test matrix produced heat transfer data for six different flow conditions. For each test condition, measurements were performed at least three times to establish repeatability. Table 3 provides the flow and heat transfer conditions for each test. The exit Reynolds number coupled with the exit Mach number is based on a vane chord and is defined by

$$\mathrm{Re}_2=\frac{\rho_2 U_2 C}{\mu_2} \tag{5}$$

where the average pressure and temperature data during the test run were used to calculate the exit Reynolds number.

Effect of Freestream Turbulence. This section discusses the effect that increasing freestream turbulence has on the heat transfer distribution over the turbine vane surface. Plots of the heat transfer distribution over the vane surface are shown in terms of the Nusselt number and the Nusselt number augmentation relative to the low freestream turbulence cases.

Figures 15–17 provide the heat transfer distributions for each freestream turbulence level at exit Mach 0.55, 0.75, and 1.01, respectively. The large scale high freestream turbulence augments the heat transfer at the leading edge, on the pressure side, and on the suction side of the vane where the boundary layer is laminar. The general shape of the heat transfer distribution over the vane surface is the same for all cases. After having achieved a relatively high heat transfer value at the leading edge, the heat transfer de-

Table 3 Test conditions for each case

	Exit Ma	Tu (%)	Exit Re	T_{o1} (°C)	$T_{\mathrm{init},w}$ (°C)
Case 1	0.55	2	900,000	105	30.4
Case 2	0.55	16	908,000	107	28.2
Case 3	0.74	2	1,050,000	102	33.4
Case 4	0.75	16	1,060,000	107	33.3
Case 5	1.02	2	1,520,000	103	29.0
Case 6	1.01	16	1,500,000	104	32.0

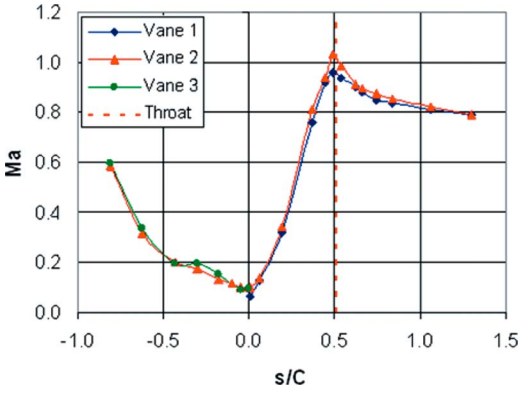

Fig. 13 Flow periodicity through vane passages

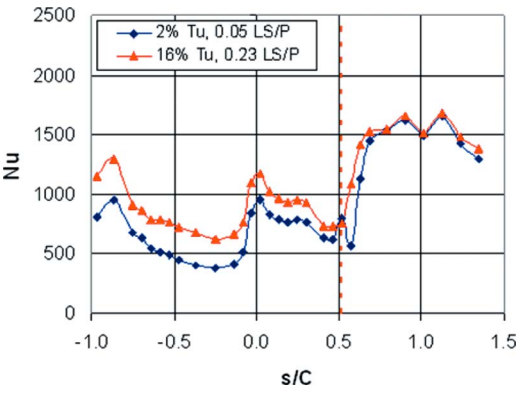

Fig. 15 Heat transfer distribution at exit Ma 0.55

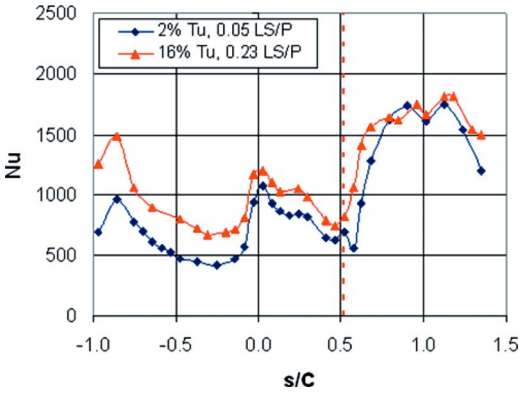

Fig. 16 Heat transfer distribution at exit Ma 0.75

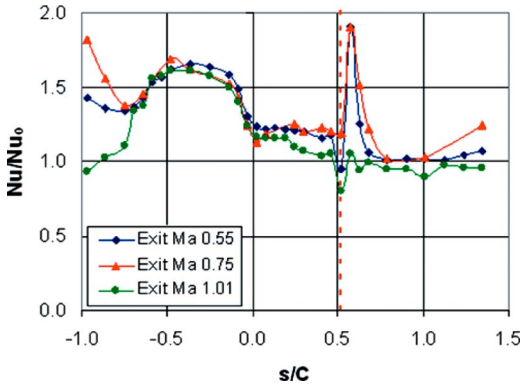

Fig. 18 Heat transfer augmentation at all exit Ma cases

creases as the flow proceeds down the suction and pressure sides due to the development of a laminar boundary layer. The heat transfer on the suction surface also responds to the pressure gradient along the surface and decreases until the boundary layer transitions, where a large increase in heat transfer occurs. The heat transfer on the pressure surface shows a decrease until $s/C=-0.25$ and then a continuous increase until $s/C=-0.86$.

On the suction side, the transition to a turbulent boundary layer occurs downstream of throat at $s/C=0.57$ for the low turbulence level at exit Mach 0.55 and 0.75. The boundary layer transition length over the vane surface is short for the exit Mach 0.55 and 0.75 cases because the flow is decelerating downstream of the throat. The boundary layer transition for the low turbulence at exit Ma 1.01 occurs at $s/C=0.40$. Since the flow is still accelerating at this point, the transition length is affected. The effect of acceleration on the transition length was also noted in the study performed by Zhang and Han [26].

The start of the transition for the high turbulence tests at exit Mach 0.55 and 0.75 appears to begin slightly earlier at $s/C=0.51$. Again, the boundary layer transition length over the vane surface is short for the exit Mach 0.55 and 0.75 cases because of flow deceleration downstream of the throat. The boundary layer transition for the high turbulence at exit Ma 1.01 occurs also at $s/C=0.40$. For the exit Mach 1.01 case, the transition location is observed to be not influenced by the large scale high freestream turbulence. The transition length for both turbulence cases at exit Mach 1.01 is interrupted around $s/C=0.57$, which corresponds to the location where trailing edge shock from the adjacent vane impinges on the suction surface. The slow transition could be attributed to the interaction of the shock with the transitioning boundary layer. Once the boundary layer goes turbulent on the suction side, the effect of the large scale high freestream turbulence level on heat transfer diminishes. This observation is consistent with Ames and Moffat [27] and Thole and Bogard [28] who showed that relatively large scale turbulence has a reduced effect on turbulent boundary layer heat transfer augmentation.

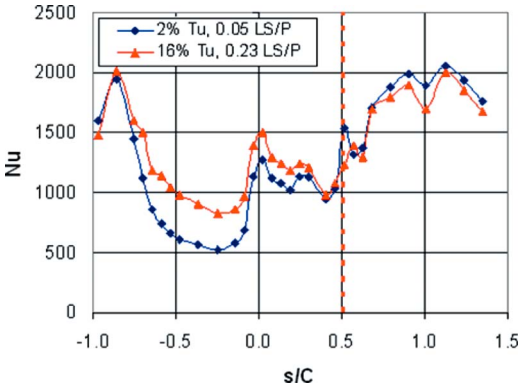

Fig. 17 Heat transfer distribution at exit Ma 1.01

The heat transfer data at high turbulence level were also normalized with the 2% turbulence data to show the augmentation levels due to turbulence. The augmentation plots for exit Mach 0.55, 0.75, and 1.01 are shown in Fig. 18. There is a peak in the augmentation plot on the suction side for the exit Mach 0.55 and 0.75 cases because the transition occurs slightly earlier than low freestream turbulence. Relatively higher augmentation levels can be seen over the majority of the pressure surface as compared to the suction surface. For instance, at exit Mach 0.75, average heat transfer augmentations of 52% and 25% were observed on the pressure and suction sides of the vane, respectively.

The heat transfer augmentation trends are similar over the majority of vane pressure surface for all exit Mach conditions. However, these augmentation plots show a change in shape at the aft end of the pressure surface. The upturn in the augmentation plot at exit Mach 0.55 and 0.75 shows a boundary layer transition behavior on the pressure surface. This upturn in the augmentation plot goes away at exit Mach 1.01, which shows that the low freestream turbulence case achieves a complete boundary layer transition on the pressure surface.

In the stagnation region, relatively lower augmentation levels are observed at exit Mach 0.75 and 1.01 than for the exit Mach 0.55 case. Since the Mach number and the Reynolds number are coupled in our facility, this behavior is consistent with the stagnation region heat transfer study of Radomsky and Thole [6] that indicates very little heat transfer augmentation with increasing Reynolds number at high freestream turbulence. The augmentation levels are similar over the majority of vane suction surface for exit Mach 0.55 and 0.75. However, at exit Mach 1.01, the augmentation level is lower in the laminar region than at exit Mach 0.55 and 0.75. This might be due to the diminishing influence of large scale high freestream turbulence on heat transfer augmentation with increasing Reynolds number.

The heat transfer data were also compared to the flat plate correlations for a laminar and turbulent boundary layer. While the flat plate correlations do not take into account the effect of pressure gradient or curvature on heat transfer, the correlations do provide insight on boundary layer behavior. The flat plate correlations reported by Incropera and DeWitt [29] in terms of the local Nusselt number are

$$\text{Laminar:}\quad \mathrm{Nu}_L = 0.332\mathrm{Re}_L^{1/2}\mathrm{Pr}^{1/3} \tag{6}$$

$$\text{Turbulent:}\quad \mathrm{Nu}_L = 0.0296\mathrm{Re}_L^{4/5}\mathrm{Pr}^{1/3} \tag{7}$$

The local Reynolds number given by

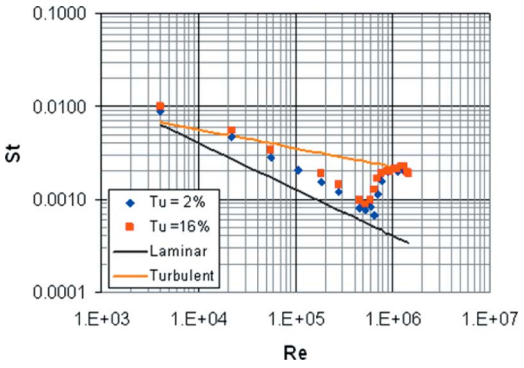

Fig. 19 Suction side data compared to the flat plate correlations at exit Ma 0.75

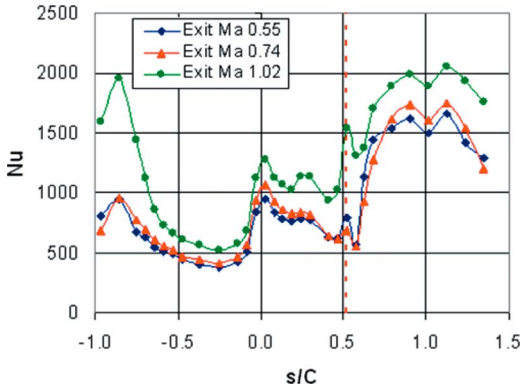

Fig. 21 Heat transfer distribution at Tu=2%

$$\mathrm{Re}_L = \frac{\rho_L U_L s}{\mu} \tag{8}$$

was used to find the Nusselt number distribution of the correlation. Averaged pressure and temperature data taken during the test run were used to calculate the local Reynolds number. The local Nusselt number was converted into a heat transfer coefficient at each measurement location by using

$$h = \frac{\mathrm{Nu}_L k_a}{s} \tag{9}$$

and then the Stanton number is calculated by using Eq. (4).

Figure 19 shows how the experimental data compare with the laminar and turbulent flat plate heat transfer correlations on the suction side of the vane at exit Mach 0.75. Before transition occurs, the boundary layer data lie between the laminar and turbulent boundary layer correlations for each case and follow the trend of laminar correlation. The difference between the laminar correlation and the low freestream turbulence data in the laminar region can be attributed to the effect of a favorable pressure gradient. The augmentation due to turbulence can also be seen on the suction side. A good agreement between the turbulent flat plate correlation and the experimental data is shown for all of the data once the flow goes turbulent on the suction surface. Similar trends were also observed for the exit Mach 0.55 and 1.01 cases.

The comparison of the experimental data at exit Mach 0.75 with the laminar and turbulent flat plate correlations on the pressure side is provided in Fig. 20. For low freestream turbulence, the data initially follow the trend of the laminar correlation and then approach the turbulent correlation toward the end of the pressure surface. At high freestream turbulence the data follow the trend of the turbulent correlation. Similar trends were also observed for exit Mach 0.55 and 1.01 cases. From the acceleration parameter in Fig. 14, the acceleration parameter barely reaches the critical value over the pressure side after $s/C=-0.43$, so there was no evidence of boundary layer relaminarization at any exit Mach condition.

Effect of Reynolds Number. The primary objective of this work was to examine the effect of freestream turbulence on heat transfer at three exit Mach number conditions. Because of this objective, the exit Mach number was not decoupled from the exit Reynolds number. An increase in exit Mach number corresponds to an increase in the exit Reynolds number. To remain consistent with the previous sections, the data will be compared by stating the Mach number. The actual exit Reynolds numbers measured for each test are provided in Table 3.

The Nusselt number distributions showing the effect of increasing the Reynolds number at turbulence levels of 2% and 16% are shown in Figs. 21 and 22, respectively. As expected, there is an overall increase in heat transfer due to the increase in Reynolds number. The increase in heat transfer level is most noticeable at the highest Reynolds number (Mach 1.01). Another effect that the highest Reynolds number has on the heat transfer is to promote an early boundary layer transition ($s/C=0.40$) on the suction side. An earlier boundary layer transition on the suction side is observed at both turbulence levels.

On the pressure side, steeper streamwise Nusselt number gradients are observed at the highest Reynolds number. These Nusselt number gradients are more noticeable at the low freestream turbulence, indicating a boundary layer transition at the aft end of the pressure side.

Leading Edge Correlation. The experimental data at the leading edge were compared to the correlation developed by Dullenkopf and Mayle [30]. The correlation takes into account the effects of freestream turbulence and integral length scale on

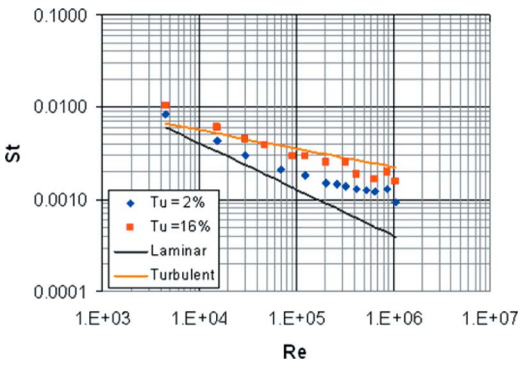

Fig. 20 Pressure side data compared to the flat plate correlations at exit Ma 0.75

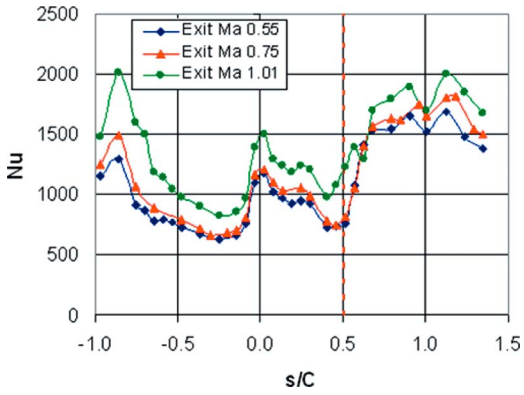

Fig. 22 Heat transfer distribution at Tu=16%

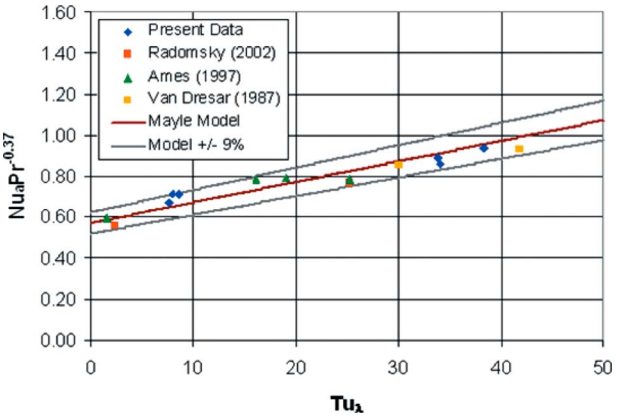

Fig. 23 Stagnation region data compared to Dullenkopf and Mayle's correlation

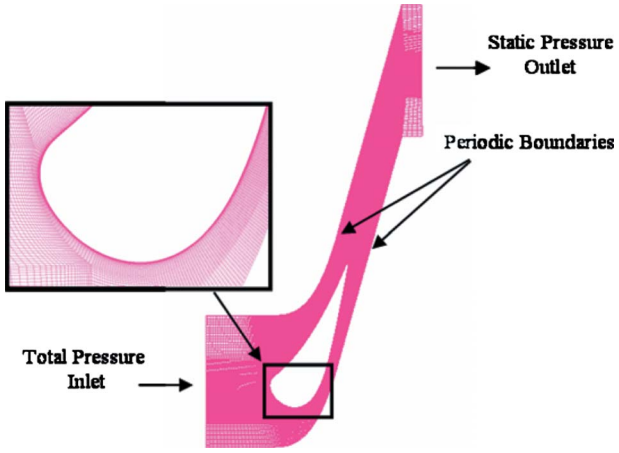

Fig. 24 Computational domain for CFD predictions

stagnation region heat transfer. The correlation requires the determination of an "effective" leading edge diameter of the vane. The effective leading edge diameter of the vane is determined by fitting the velocity distribution around the suction side of the vane to a potential flow theory for a cylinder in crossflow. The correlation uses an effective turbulence level and also takes into account the strain rate. The effective Nusselt number is presented as a function of this effective turbulence level Tu_λ by

$$Nu_a Pr^{-0.37} = 0.571 + 0.01 Tu_\lambda \tag{10}$$

where

$$Nu_a = \frac{Nu_D}{\sqrt{a_1 Re_D}} \tag{11}$$

and the value of Tu_λ is determined by

$$Tu_\lambda = \frac{Tu_a \sqrt{L_a}}{(1 + 0.004 L_a^2)^{5/12}} \tag{12}$$

The dimensionless length scale L_a is given by

$$L_a = (\Lambda_x / D) \sqrt{a_1 Re_D} \tag{13}$$

and

$$Tu_a = Tu \sqrt{a_1 Re_D} \tag{14}$$

It must be mentioned that the dimensionless strain rate $a_1 = 4$ was used for the stagnation data. Figure 23 shows the comparison of current heat transfer data and the previous literature investigations [4,6,31] with Dullenkopf and Mayle's correlation for stagnation region heat transfer. The experimental data at the leading edge compare rather well with the correlation. All of the data follow the same trend as the correlation and lies within $\pm 9\%$ (bias error) of the correlation.

FLUENT and TEXSTAN Comparison. Computational fluid dynamics (CFD) heat transfer predictions at low freestream turbulence were performed using a commercially available software package (FLUENT 6.2.6). A 2D computational domain representing one full vane passage with periodic boundary conditions was employed to simulate the cascade test condition. The computational inlet was located at 0.45C upstream of the vane leading edge. For all test cases, total pressure and total temperature were specified at the inlet and static pressure was specified at the outlet. The vane geometry was simulated with constant wall temperature boundary condition. Freestream turbulence level and length scale were also specified at the inlet for all test cases. Fluid specific heat, thermal conductivity, and molecular viscosity were kept constant for all test cases.

For the FLUENT solver, a coupled implicit solution method with the second-order upwind discretization scheme was chosen. The Reynolds-averaged Navier-Stokes (RANS) based v^2-f turbulence model, originally suggested by Durbin [32], was used in all numerical predictions. A 2D hexahedral mesh consisted of 73,300 cells and was refined near the wall to better capture wall heat transfer, as shown in Fig. 24. This was achieved by adjusting the near-wall spacing y^+ to be less than 1. The convergence of calculation was assumed to be reached when all normalized residuals were smaller than 10^{-5}, except energy smaller than 10^{-7}. In general, 3000 iterations were required for full convergence.

Figure 25 shows the comparison of predicted and measured Mach number distributions around the vane surface for three exit Mach number conditions. Overall, the FLUENT results compare very well with the experimental data on the pressure side at all exit Mach conditions. On the suction side, the FLUENT predictions also compare well with the experimental data at exit Mach 0.6 and 0.8. For the exit Mach 1.0 case, the FLUENT prediction matches the experimental data up to $s/C = 0.58$, but then the FLUENT model is unable to reasonably predict multiflow decelerations caused by the shock wave on suction side Mach number distribution.

Figures 26–28 provide the comparison of measured and predicted Nusselt number distributions for low freestream turbulence levels at exit Mach 0.55, 0.75, and 1.01, respectively. The v^2-f model compares generally well over the majority of the vane pressure surface at all exit Mach conditions, as observed by other authors [33,34]. The model overpredicts the heat transfer at the leading edge and in the laminar region on the suction side for the exit Mach 0.55 and 0.75 cases. The v^2-f model also predicts an early boundary layer transition on the suction side and overpredicts the heat transfer at the end of transition for the exit Mach 0.55 and 0.75 cases. An early boundary layer prediction and over-

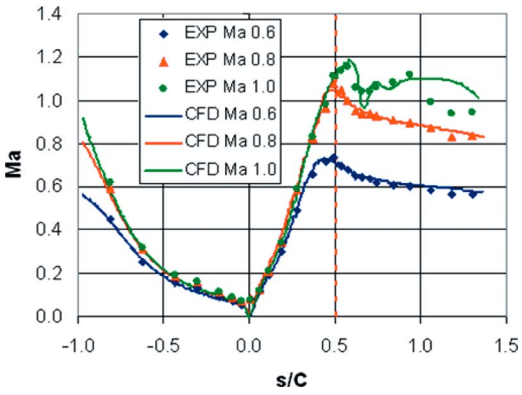

Fig. 25 Local Mach number distribution comparison

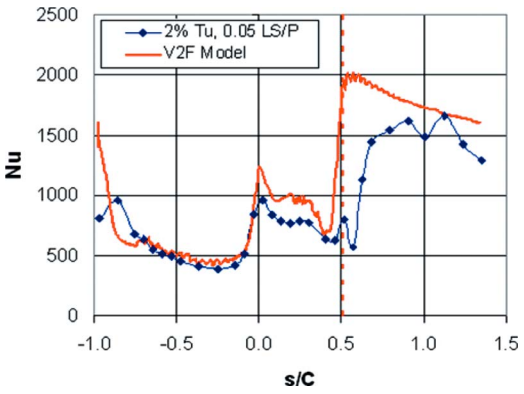

Fig. 26 FLUENT prediction at exit Ma 0.55, 2% Tu

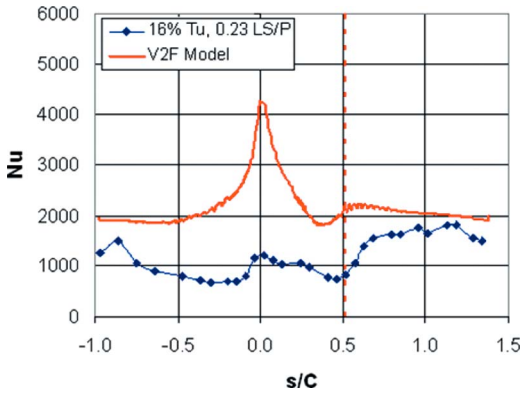

Fig. 29 FLUENT prediction at exit Ma 0.75, 16% Tu

prediction of the heat transfer at the end of transition has also been observed by Luo and Razinsky [34]. At exit Mach 1.01, the v^2-f model overpredicts heat transfer at the leading edge but then underpredicts it in the region from $s/C=0.25$ to $s/C=0.5$. Also the v^2-f model underpredicts turbulent boundary layer heat transfer on the suction and pressure sides of the vane at exit Mach 1.01.

An attempt was also made to perform FLUENT v^2-f heat transfer predictions at high freestream turbulence level but the v^2-f model profoundly overpredicted heat transfer at high freestream turbulence on the entire surface of the vane at all exit Mach conditions. Figure 29 provides a comparison of measured and predicted Nusselt number distributions for a high freestream turbulence level at exit Mach 0.75. The leading edge heat transfer is profoundly overpredicted and seems to affect the heat transfer levels on the entire surface of the vane. Modeling freestream turbulence eddy viscosity as a function of large length scale, proper scaling of high freestream turbulence near the wall, and developing correct models to account for the heat transfer augmentation in the leading edge region and both surfaces of the vane at high freestream turbulence are challenging and require more work.

The experimental data were also compared with the numerical predictions of an academic version of TEXSTAN developed by Crawford [35]. To model the flow through the vane passages, the two-equation Lam–Bremhorst turbulence model was used with the Schmidt–Patankar transition model. A constant surface temperature boundary condition was applied to the vane, and the constant freestream turbulence kinetic energy was set throughout the computational domain by freezing the turbulence dissipation rate.

At low freestream turbulence, the TEXSTAN predictions match well with the experimental data at all exit Mach conditions on the pressure side until $s/C=-0.53$ but then start to deviate from the measurements, as shown in Figs. 30–32. On the suction side, the predictions match well with the data in the laminar region downstream of the leading edge, but the above mentioned turbulence and transition models did not predict boundary layer transition. For the low freestream turbulence case at all exit Mach conditions only, the TEXSTAN was forced to transition at the location where the experimental data indicated transition by using an abrupt transition model.

At high freestream turbulence, TEXSTAN overpredicted the heat transfer on both the pressure and suction sides of the vane at all exit Mach conditions, as shown in Figs. 33–35. The leading edge heat transfer is also overpredicted at all exit Mach conditions. However, the suction side predictions show a similar trend in the laminar region, with the data only coming close to the prediction after the transition. The pressure side predictions at all exit Mach conditions also show a similar trend, with the data coming close to prediction at the aft end of the pressure surface.

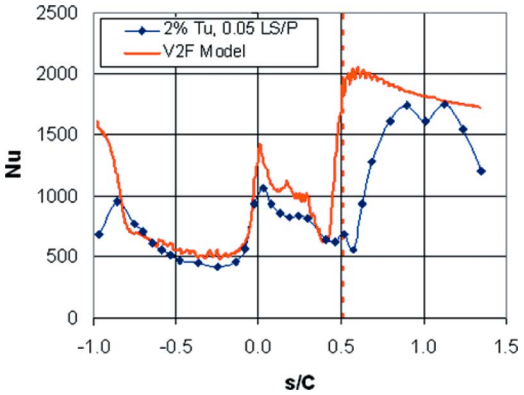

Fig. 27 FLUENT prediction at exit Ma 0.75, 2% Tu

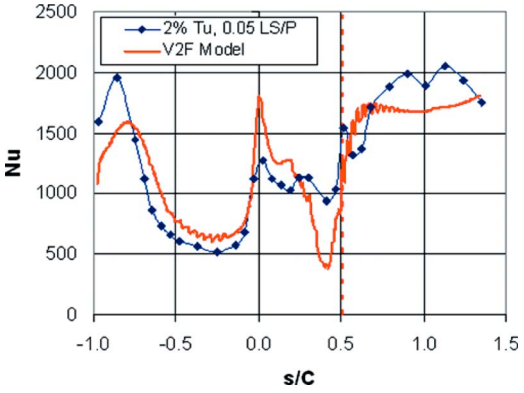

Fig. 28 FLUENT prediction at exit Ma 1.01, 2% Tu

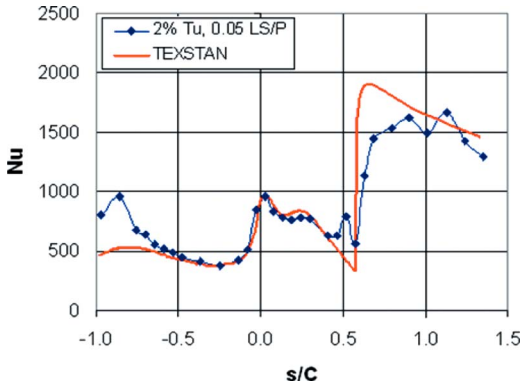

Fig. 30 TEXSTAN prediction at exit Ma 0.55, 2% Tu

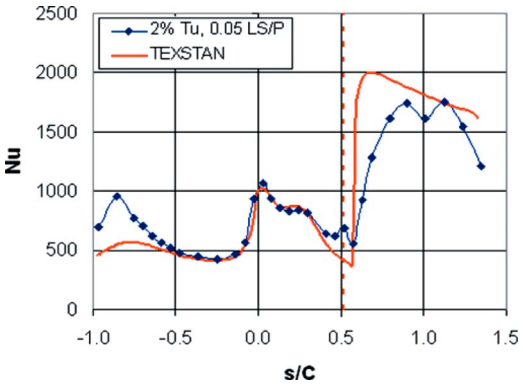

Fig. 31 TEXSTAN prediction at exit Ma 0.75, 2% Tu

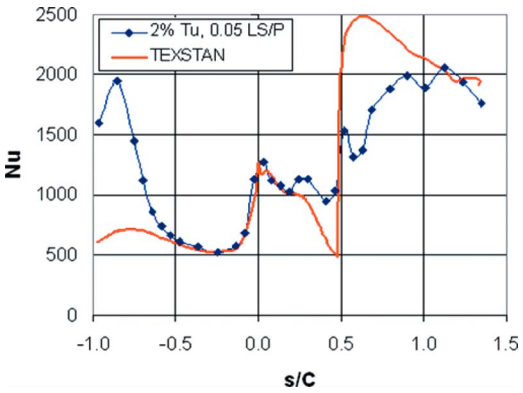

Fig. 32 TEXSTAN prediction at exit Ma 1.01, 2% Tu

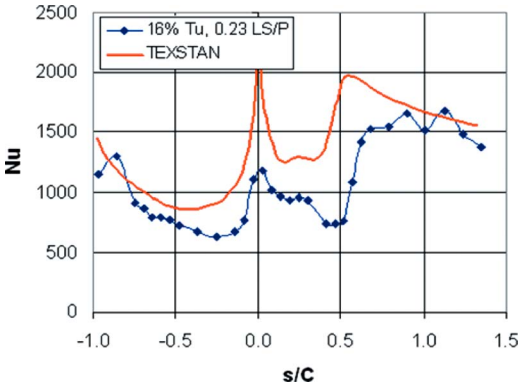

Fig. 33 TEXSTAN prediction at exit Ma 0.55, 16% Tu

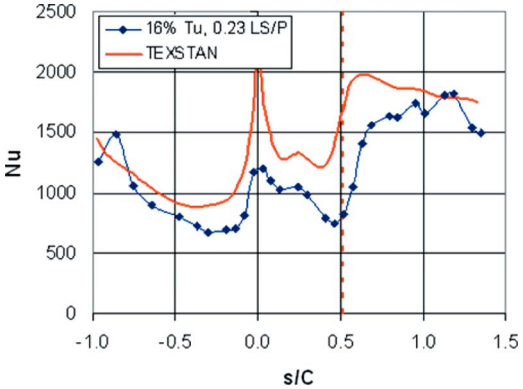

Fig. 34 TEXSTAN prediction at exit Ma 0.75, 16% Tu

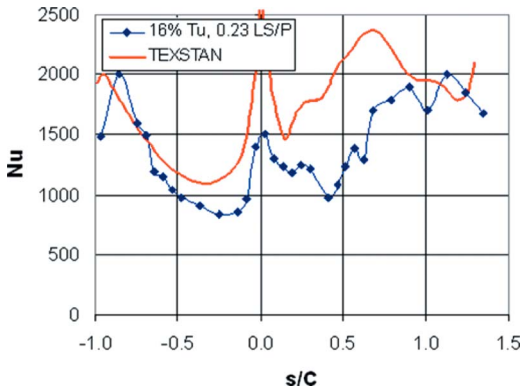

Fig. 35 TEXSTAN prediction at exit Ma 1.01, 16% Tu

Conclusions

Aerodynamic and heat transfer measurements were made on a turbine vane at flow conditions representative of engine operating conditions. Large scale high freestream turbulence was generated by using a passive turbulence grid. Increasing the turbulence level was observed to augment the heat transfer over the vane surface.

Relatively higher augmentation levels were seen over the majority of the pressure surface as compared to the suction surface for all exit Mach conditions. High freestream turbulence hastened the boundary layer transition on the suction side for the exit Mach 0.55 and 0.75 cases. For the exit Mach 1.01 case, the turbulence augmentation was small on the suction surface as compared to the exit Mach 0.55 and 0.75 cases. Also for the exit Mach 1.01 case, increasing the freestream turbulence was observed to not influence the location of boundary layer transition on the suction surface.

As expected, increasing the exit Reynolds number was shown to increase the heat transfer levels and cause earlier boundary layer transition on the suction side for the highest Reynolds number (1.5×10^6). On the pressure side, steeper streamwise Nusselt number gradients were observed at the highest Reynolds number. These Nusselt number gradients were more noticeable at the low freestream turbulence, indicating a boundary layer transition to turbulent flow at the aft end of the pressure side.

Several comparisons were made between the data using the analytical flat plate correlations, leading edge correlation developed by Dullenkopf and Mayle [30], FLUENT v^2-f model, and TEXSTAN predictions. The heat transfer data showed a good agreement with flat plate and leading edge correlations. The v^2-f model, and TEXSTAN resulted in an overall reasonable prediction of the heat transfer at low freestream turbulence levels. At high freestream turbulence, FLUENT v^2-f model and TEXSTAN was found to significantly overpredict the heat transfer levels on the vane surface.

Acknowledgment

This work was sponsored by Solar Turbines Inc. We would also like to express our gratitude to Dr. Richard Anthony and Dr. Marcus Polanka of the Air Force Research Laboratory, Wright-Patterson AFB for their help with manufacturing and implementation of the thin film gauges. Laboratory, Wright-Patterson AFB for their help with the manufacturing and implementation of the thin film gauges.

Nomenclature

a_1 = dimensionless strain rate
B = bar width of turbulence grid
C = vane chord
C_p = constant pressure specific heat
D = effective leading edge diameter of vane
f = elliptic operator in the V2F model

h = heat transfer coefficient
k_a = thermal conductivity of air
k = acceleration parameter/thermal conductivity/turbulent kinetic energy
L_a = dimensionless length scale
LS = integral turbulence length scale
Ma = Mach number
Nu = Nusselt number
Nu_a = effective Nusselt number
Nu_0 = Nusselt number at Tu=2%
Nu_D = Nusselt number based on D
P = vane pitch
Pr = Prandtl number
q'' = heat flux
r_c = recovery factor
Re = Reynolds number
Re_D = Reynolds number based on D, evaluated at inlet conditions
s = vane surface distance from stagnation point
St = Stanton number
T = temperature
Tu = streamwise freestream turbulence intensity
Tu_a = modified turbulence intensity
Tu_λ = effective turbulence intensity
U = local velocity
v^2 = wall normal Reynolds stress component
x = streamwise distance from turbulence grid
y^+ = equivalent normal distance

Greek

γ = specific heat ratio of air
Λ_x = integral turbulence length scale
ρ = local density of air
μ = dynamic viscosity of air

Subscripts

1, 2 = inlet conditions, exit conditions
aw, w = adiabatic wall, wall
gauge = thin film gauge (surface) measurement
init = initial
L = local conditions
o = stagnation

References

[1] Zimmermann, D. R., 1979, "Laser Anemometer Measurements at the Exit of a T63-C20 Combustor," NASA Report No. CR-159623.
[2] Van Fossen, G. J., and Bunker, R. S., 2001, "Augmentation of Stagnation Heat Transfer Due to Turbulence From a DLN Can Combustor," ASME J. Turbomach., **123**, pp. 140–146.
[3] Ames, F. E., Wang, C., and Barbot, P. A., 2003, "Measurement and Prediction of the Influence of Catalytic and Dry Low NO_x Combustor Turbulence on Vane Surface Heat Transfer," ASME J. Turbomach., **125**, pp. 221–231.
[4] Ames, F. E., 1997, "The Influence of Large-Scale High Intensity Turbulence on Vane Heat Transfer," ASME J. Turbomach., **119**, pp. 23–30.
[5] Ames, F. E., Argenziano, M., and Wang, C., 2004, "Measurement and Prediction of Heat Transfer Distributions on an Aft Loaded Vane Subjected to the Influence of Catalytic and Dry Low NO_x Combustor Turbulence," ASME J. Turbomach., **126**, pp. 139–149.
[6] Radomsky, R., and Thole, K. A., 2002, "Detailed Boundary Layer Measurements on a Turbine Stator Vane at Elevated Freestream Turbulence Levels," ASME J. Turbomach., **124**, pp. 107–118.
[7] Nealy, D. A., Mihelc, M. S., Hylton, L. D., and Gladden, H. J., 1990, "Measurements of Heat Transfer Distribution Over the Surfaces of Highly Loaded Turbine Nozzle Guide Vanes," ASME J. Eng. Gas Turbines Power, **106**, pp. 149–158.
[8] Arts, T., and Lambert de Rouvroit, M., 1992, "Aero-Thermal Performance of a Two-Dimensional Highly Loaded Transonic Turbine Nozzle Guide Vane: A Test Case for Inviscid and Viscous Flow Computations," ASME J. Turbomach., **114**, pp. 147–154.
[9] Hoffs, A., Drost, U., and Bolcs, A., 1996, "Heat Transfer Measurements on a Turbine Airfoil at Various Reynolds Numbers and Turbulence Intensities Including Effects of Surface Roughness," ASME Paper No. GT-1996-169.
[10] Bunker, R. S., 1997, "Separate and Combined Effects of Surface Roughness and Turbulence Intensity on Vane Heat Transfer," ASME Paper No. GT-1997-135.
[11] Carullo, J. S., Nasir, S., Cress, R. D., Ng, W. F., Thole, K. A., Zhang, L. J., and Moon, H. K., 2007, "The Effects of Freestream Turbulence, Turbulence Length Scale, and Exit Reynolds Number on Turbine Blade Heat Transfer in a Transonic Cascade," ASME Paper No. GT-2007-27859.
[12] Nix, A. C., Diller, T. E., and Ng, W. F., 2007, "Experimental Measurements and Modeling of the Effects of Large-Scale Freestream Turbulence on Heat Transfer," ASME J. Turbomach., **129**, pp. 542–550.
[13] Holmberg, D. G., and Diller, T. E., 2005, "Simultaneous Heat Flux and Velocity Measurements in a Transonic Turbine Cascade," ASME J. Turbomach., **127**, pp. 502–506.
[14] Smith, D. E., Bubb, J. V., Popp, O., Grabowski, H. C., Diller, T. E., Schetz, J. A., and Ng, W. F., 2000, "An Investigation of Heat Transfer in a Film Cooled Transonic Turbine Cascade—Part I: Steady Heat Transfer," ASME Paper No. 2000-GT-202.
[15] Popp, O., Smith, D. E., Bubb, J. V., Grabowski, H. C., Diller, T. E., Schetz, J. A., and Ng, W. F., 2000, "An Investigation of Heat Transfer in a Film Cooled Transonic Turbine Cascade—Part II: Unsteady Heat Transfer," ASME Paper No. 2000-GT-203.
[16] Schultz, D. L., and Jones, T. V., 1973, "Heat Transfer Measurements in Short Duration Hypersonic Facilities," AGARD Paper No. AG-165.
[17] Doorly, J. E., and Oldfield, M. L. G., 1987, "The Theory of Advanced Multi-Layer Thin Film Heat Transfer Gages," Int. J. Heat Mass Transfer, **30**, pp. 1159–1168.
[18] Dunn, M. G., 1995, "The Thin-Film Gage," *Von Karman Institute for Fluid Dynamics Lecture Series 1995*.
[19] Joe, C. R., 1997, "Unsteady Heat Transfer on the Turbine Research Facility at Wright Laboratory," Ph.D. thesis, Syracuse University.
[20] Cress, R. D., 2006, "Turbine Blade Heat Transfer Measurements in a Transonic Flow Using Thin Film Gages," MS thesis, Virginia Polytechnic Institute and State University.
[21] Moffat, R. J., 1988, "Describing Uncertainties in Experimental Results," Exp. Therm. Fluid Sci., **1**, pp. 3–17.
[22] Baines, W. D., and Peterson, E. G., 1951, "An Investigation of Flow Through Screens," Trans. ASME, **73**, pp. 467–480.
[23] Nix, A. C., Smith, A. C., Diller, T. E., Ng, W. F., and Thole, K. A., 2002, "High Intensity, Large Length-Scale Freestream Turbulence Generation in a Transonic Turbine Cascade," ASME Paper No. GT-2002-30523.
[24] Jones, W. P., and Launder, B. E., 1972, "The Prediction of Laminarization With a Two-Equation Model of Turbulence," Int. J. Heat Mass Transfer, **15**, pp. 301–314.
[25] Mayle, R. E., 1991, "The Role of Laminar-Turbulent Transition in Gas Turbine Engines," ASME J. Turbomach., **113**, pp. 509–537.
[26] Zhang, J., and Han, J.-C., 1994, "Influence of Mainstream Turbulence on Heat Transfer Coefficient From a Gas Turbine Blade," ASME J. Heat Transfer, **116**, pp. 896–903.
[27] Ames, F. E., and Moffat, R. J., 1990, "Heat Transfer With High Intensity, Large Scale Turbulence: The Flat Plate Turbulent Boundary Layer and the Cylindrical Stagnation Point," Thermosciences Division of Mechanical Engineering, Stanford University, Report No. HMT-44.
[28] Thole, K. A., and Bogard, D. G., 1995, "Enhanced Heat Transfer and Skin Friction Due to High Freestream Turbulence," ASME J. Turbomach., **117**, pp. 418–424.
[29] Incropera, F. P., and DeWitt, D. P., 2002, *Fundamentals of Heat and Mass Transfer*, 5th ed., Wiley, New York.
[30] Dullenkopf, K., and Mayle, R. E., 1995, "An Account of Free-Stream-Turbulence Length Scale on Laminar Heat Transfer," ASME J. Turbomach., **117**, pp. 401–406.
[31] Van Dresar, N. T., and Mayle, R. E., 1989, "A Quasi-Steady Approach to Leading Edge Heat Transfer Rates," ASME J. Turbomach., **111**, pp. 483–490.
[32] Durbin, P., 1991, "Near-Wall Turbulence Closure Modeling Without 'Damping Functions'," Theor. Comput. Fluid Dyn., **3**, pp. 1–13.
[33] Pecnik, R., Pieringer, P., and Sanz, W., 2005, "Numerical Investigation of the Secondary Flow of a Transonic Turbine Stage Using Various Turbulence Closures," ASME Paper No. GT-2005-68754.
[34] Luo, J., and Razinsky, E. H., 2007, "Conjugate Heat Transfer Analysis of a Cooled Turbine Vane Using the v^2-f Turbulence Model," ASME J. Turbomach., **129**, pp. 773–781.
[35] Crawford, M. E., 1986, "Simulation Codes for Calculation of Heat Transfer to Convectively-Cooled Turbine Blades," *A Set of Four Lectures in Convective Heat Transfer and Film Cooling in Turbomachinery VKI Lecture Series* 1986.